The EMPIR initiative is co-funded by the European Union's Horizon 2020 research and innovation programme and the EMPIR Participating States

15RPT01 RFMicrowave, D5

Report on Support Effects on EMC Test Results in Both Emission and Immunity Tests Using a VNA

Project Number: 15RPT01

Project Title: Development of RF and microwave metrology capability

Document Type: Deliverable report (D5)

Authors: Osman Şen, Soydan Çakır, Murat Celep, Marc Pous, Ferran Silva, Savaş Acak, Borut Pinter, Urban Lundgren

Activity Partners: TÜBİTAK UME, UPC, SIQ, RISE

Due date of the deliverable: Jan 2018

Submission date: Feb 2018

CONTENTS

1. SUMMARY

This report was prepared to present the investigation results of the effects of supports on both emission and immunity tests by using a Vector Network Analyser (VNA). While the “Conducted Tests” part (Section 2) of this report was performed and prepared by TUBITAK UME, the “Radiated Tests” & “EM Simulation” parts (Section 3 & Section 4) were performed and prepared by UPC. The literature study was performed by RISE and SIQ.

2. CONDUCTED TESTS

a. Introduction

The conducted immunity test is one of the major EMC immunity tests and widely performed in laboratories in the frequency range 150 kHz - 80 MHz by the use of CDNs in accordance with IEC61000-4-6 [1] and sometimes is extended to 230 MHz. The principle of the test is to induce electric and magnetic disturbance inside the Equipment Under Test (EUT) by applying a conducted disturbance signal in Common Mode (CM) on the EUT input and output cables. The disturbance is applied via a defined source impedance of 150 Ω. A piece of good work on deep details of the conducted immunity test and its advantages / disadvantages is perfectly presented in [2]. In addition, pitfalls and practice of conducted immunity testing were very well studied in [3]. There are also a few more researches on application of the standard IEC61000-4-6 in the literature. Some of them give useful information for the enhancement of standard applications such as automation and speeding up of the tests [4-5]. The others focus on investigation and comparison of some conducted immunity test components such as EM and Bulk Current Injection (BCI) clamps in terms of tests and calibrations [6-7]. Practical approach to IEC61000-4-6 and variations in injected currents are studied in [8-9]. Finally, alternative conducted immunity test applications for industry, which are based on loop impedance measurements, were studied and loop impedance measurements were included into conducted immunity researches for the first time in [10,11].

In this work, we bring the current state-of-the-art research one more step further and investigate details and pitfalls of conducted immunity laboratory setups in more detail by analyzing loop impedance values and injected currents with the inclusion of different supports which are utilized to isolate EUTs from the ground plane as stipulated by the standard. In fact, support effects on radiated emission tests were investigated in several papers such as [12] but it is studied for conducted immunity tests for the first time in this work. As supports, we included four materials; wood, molding polyamide, styrofoam and

copper. For loop impedance measurements, although there are some methods in the literature, we chose the two current probe method introduced in [13] for our research.

b. Theory and experimental setup

The deep investigation of the conducted immunity test and support influences on it in our research is completely based on the impedance measurements of loop impedance values from 150 kHz to 230 MHz. The loop impedance measurement method that we used is stated in [13] in detail. This impedance measurement method uses a Vector Network Analyzer (VNA), two current probes and a piece of precision known impedance. It yields the value of the unknown target impedance as well as the overall loop impedance. The standard IEC61000-4-6 requires the test setup presented in Fig.1. As seen in Fig.1, the loop impedance includes two 150 Ohm impedance values formed by CDNs and the EUT on the loop [10]. As measured impedance values by the VNA are complex numbers, the correction factor K becomes a complex number. On all the impedance graphs in this work, we only give the module values of the complex numbers. The injected power is obtained in the calibration phase in a test jig before the test, as stated in IEC61000-4-6.

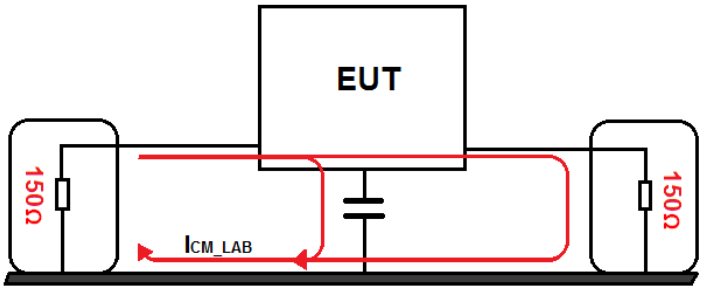

Figure 1. Conducted immunity test setup [10].

(a) (b)

Figure 2. (a) Setup for repeatability verification, (b) supports used in research.

After modeling the test setups, as seen in Fig.2 (a), we firstly performed some repeatability checks of the loop impedance measurements on a simple setup which was installed with a simple metallic structure and the supports beneath three times per non-conductive support on different occasions. Following the verification of the repeatability, we continued the measurements with the thermo-hygrometer along with the insulation supports under investigation. The thermo-hygrometer was modified and specially made susceptible to RF disturbances. As insulation supports, we utilized four support types with a height of 10 cm and seen in Fig.2 (b); styrofoam, molding polyamide, wood and a copper-wrapped one. It must be specially stated here that the metallic supports are not normally required by any standard however the metallic support was used to present the worst case situation and to show the efficiency and performance of the loop impedance measurement in the extreme condition. After the test setup was established, the loop impedance of the setup with each support in turn was measured with a frequency step size of 250 kHz by using the two-probe impedance measurement method. After the measurement of the loop impedance values of the setups, the EUT was actually tested in the laboratory setup with the CDN, which contains each support in turn, as seen in Fig.3 (a). The two probes utilized for loop impedance measurement were also kept in place in the test phase in order to maintain consistency between the loop impedance measurement and the test. In addition, the receiving current probe used in the impedance measurement was also used to measure the injected current and the injection probe used in the impedance measurement was terminated with 50 Ohm in the test stage. Thereafter the calibrated power level was applied to the RF input port of the CDN of the setup and the current injected into the loop was experimentally measured by the receiving probe. During the tests, the current injected to the setup and the susceptibility of the EUT, which corresponds to the temperature/humidity deviation caused by injected disturbance on its display, were recorded to be compared to each other in an attempt to link the loop impedance measurement results to the susceptibility results of the EUT. The thermo-hygrometer was powered as intended and was connected to the mains through a M2 CDN in the power port as seen in Fig.3 (a). The deviation in the laboratory temperature, subsequently in the read value on the display of the thermometer, between the beginning and the end of the measurements in the absence of the disturbance signal was recorded approximately as $0.5^{o}C$, consequently the effect of the change in the laboratory temperature on the measurement results was assumed to be negligible. On the other hand, it was not easy to control the humidity of the test chamber during a whole long test and we accordingly normalized the natural laboratory humidity deviations which did not result from the disturbance signal.

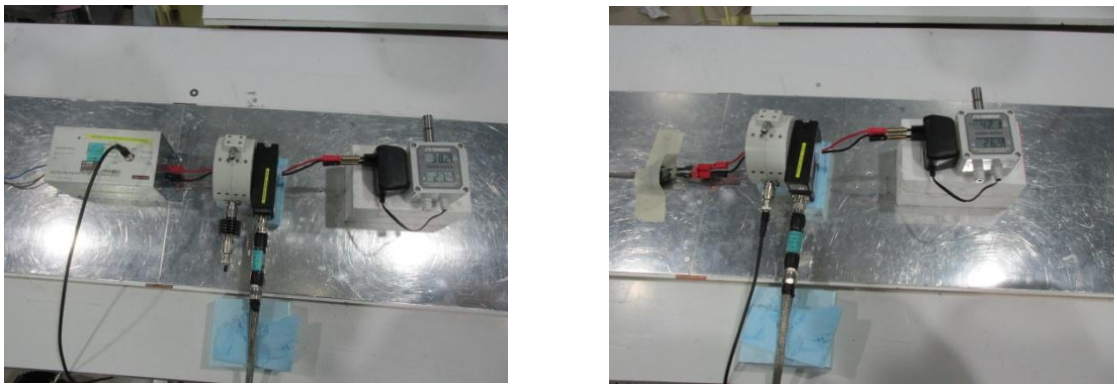

(a) (b)

Figure 3. Conducted immunity test setups of the electronic thermometer (a) with CDN, (b) with mains without CDN.

As it is not always possible to use CDNs due to some limitations such as high supply currents especially in industrial environments, we also studied the support effects for the case without the CDN. In this final step, we tested the EUT connected directly to the mains without the CDN as seen in Fig.3 (b) and the injection was performed by means of the BCI clamp, which had been also used for the loop impedance measurement. Finally, in addition to the measurement of the samples in actual tests, S-parameters of wood, molding polyamide and white styrofoam materials at a high frequency, 2 GHz, were measured by using a WR 430 waveguide. The reference points were defined before the measurement of each material, thereafter measurements were performed according to the setup given in Fig. 4. In this setup, the errors of the vector network analyzer were corrected using the Thru Reflect Line (TRL) calibration model. The measured samples were tightly placed in a waveguide in turn in such a way that each sample fully covered the inner section of the waveguide. The waveguide WR 430 was connected between the two measurement ports of the VNA and the S-parameters were measured. The dielectric coefficient of each sample was calculated by means of the Nicolson-Ross method and by using the measured magnitude and phase of the S_{11} and S_{21} parameters [14].

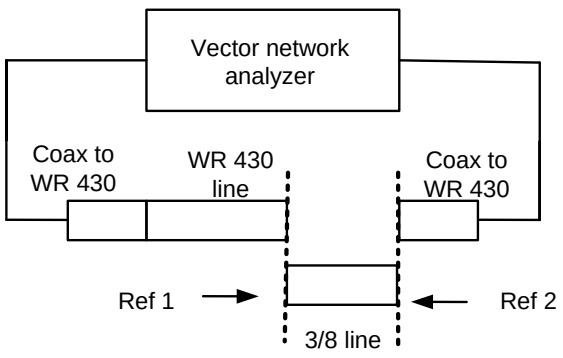

Figure 4. S–parameter measurement set-up for calculating dielectric constant at 2 GHz.

c. Experimental results and discussions

The repeatability of the loop impedance results is presented in Fig.5. While Fig.5 (a) shows the overall 9 measurements in one graph, Fig.5 (b) zooms in on the resonance regions of the curves to show the repeatability in more detail. The repeatability of loop impedance results looks very satisfactory per support within maximum ± 5 Ohms.

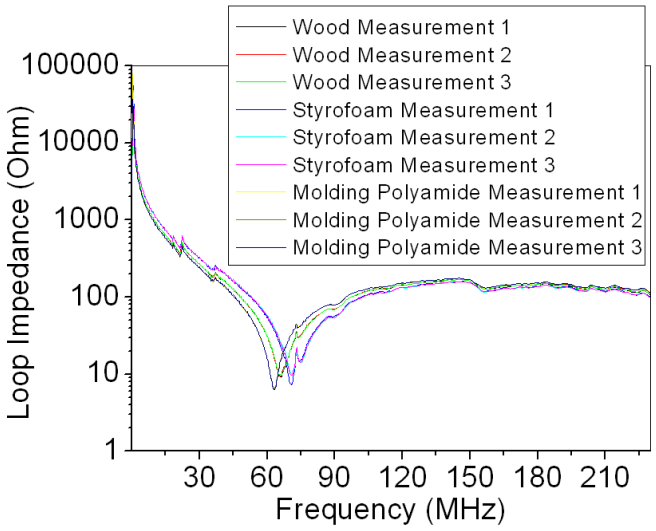

(a)

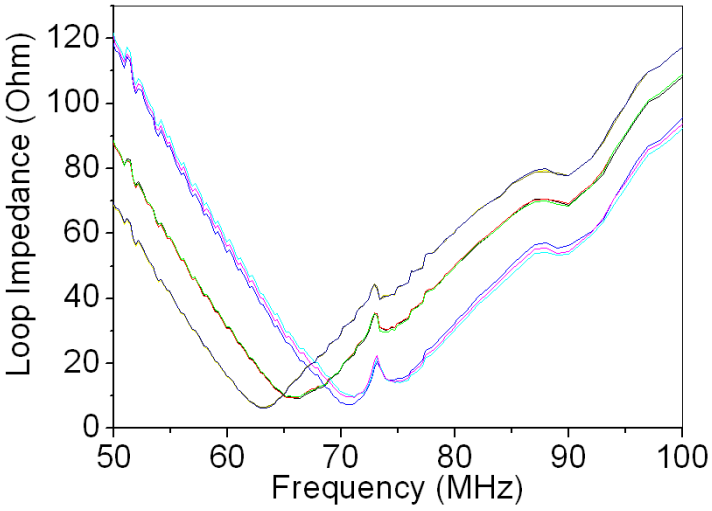

(b)

Figure 5. Repeatability verification (a) full frequency range, (b) zoomed in.

The loop impedance measurement results for the setup with the thermo-hygrometer connected to the CDN and placed on each support in turn are presented in Fig.6 (a). As seen in Fig.6 (a), the support effects on the loop impedance are clearly noticeable. Although it is

not easily observable in the graph due to the large scale of the graph, the loop impedance of the setup with the styrofoam support is generally higher than the setups with the wood and molding polyamide supports in most of the frequency range. On the other hand, the loop impedance values of the setups with the wood and styrofoam supports look similar. The loop impedance values of the setup with the EUT placed on a copper-wrapped support are lower than all the others in most of the frequency range as expected but it is surprisingly higher than the other curves in some small frequency ranges. The graph seen in Fig.6 (b) reveals that the current injected into the loop is inversely proportional to the loop impedance as expected. For example, in the frequency range up to 90 MHz, while the loop impedance of the setup with the copper-wrapped support is significantly lower than the others, the consequent current injected to the loop is higher than the others in this lower frequency range. The similar behaviour of the current and the loop impedance is easily seen in the other frequency ranges. Regarding the susceptibility, the EUT is affected in different frequency ranges in terms of the temperature and humidity display deviations. For the displayed temperature, the EUT is severely affected by the injected interference in the broad frequency range from 30 MHz to 180 MHz. On the other hand, for the displayed humidity deviations, the frequency range in which the EUT is affected is smaller and concentrated around 160 MHz. Although the frequency ranges are different, there is a reasonably good relation between the injected current level and the susceptibility of the EUT in the frequency ranges where the EUT is affected. Generally, as the injected current increases, the severity of the failure of the EUT increases. In this context, while the copper-wrapped support causes the most severe deviation on the EUT display in most of the effective frequency range, the styrofoam support causes the least effect, which is compatible with the impedance and injected current curves. The molding polyamide and wood supports have similar effects on the test results but their effects on the test results are clearly different from the effects of the styrofoam as seen in Fig.6 (c). While the EUT is affected similarly for wood and molding polyamide, the effects on the EUT are markedly reduced with the use of the styrofoam support. This means that any non-conductive support with a higher dielectric constant may result in higher effects on the conducted immunity test results in comparison to the styrofoam support or air. These first results are very essential to show the direct effects of the supports on the loop impedance and test results and to gain more insight into details of conducted immunity tests.

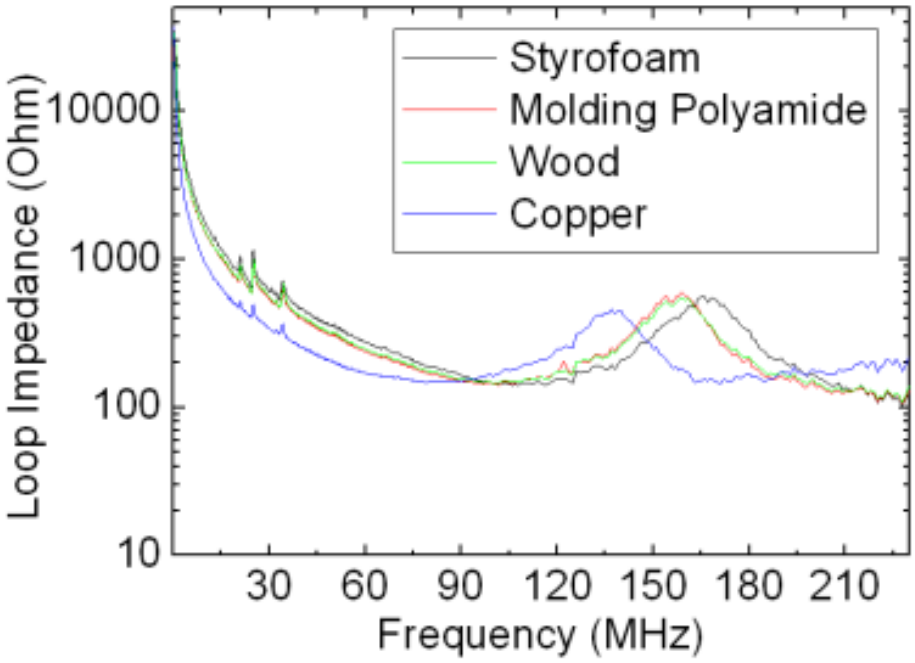
Loop Impedance (Ohm)
10000
1000
100
10
30
60
90
120
150
180
210
Frequency (MHz)
Styrofoam
Molding Polyamide
Wood
Copper

(a)

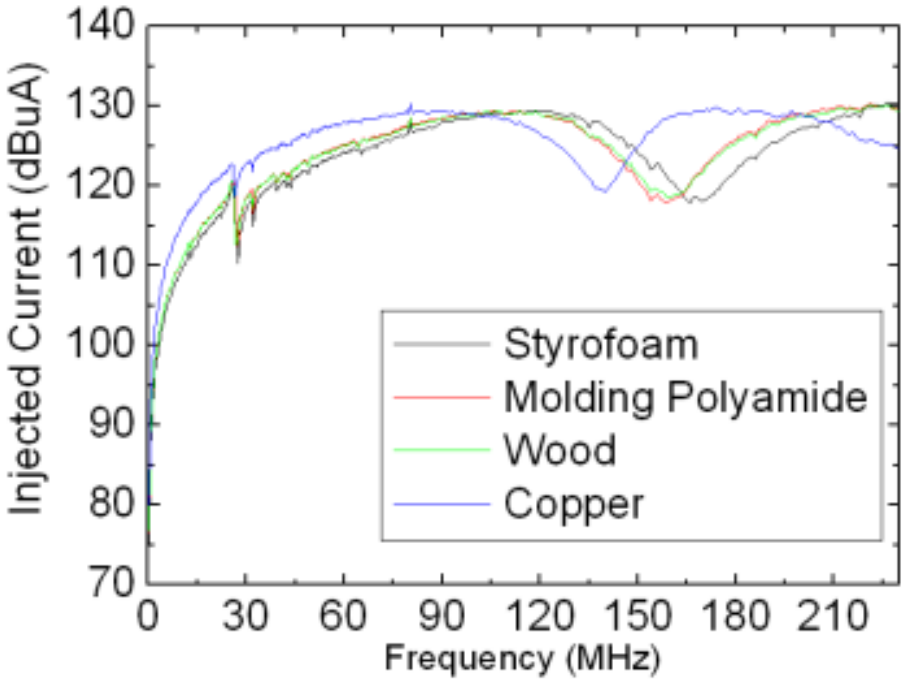
Injected Current (dBuA)
140
130
120
110
100
90
80
70
0
30
60
90
120
150
180
210
Frequency (MHz)
Styrofoam
Molding Polyamide
Wood
Copper

(b)

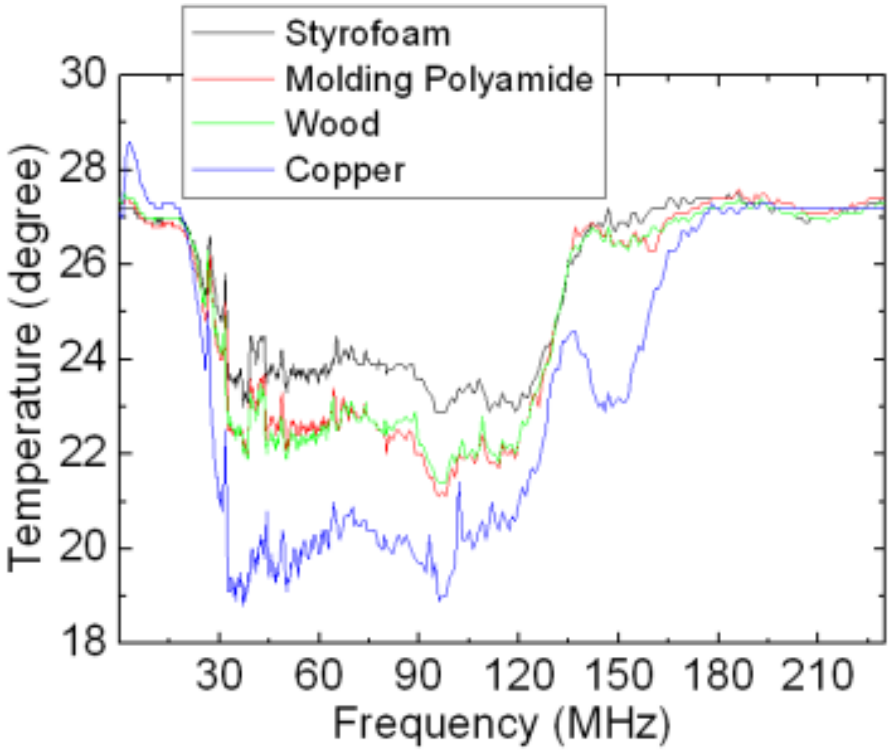

(c)

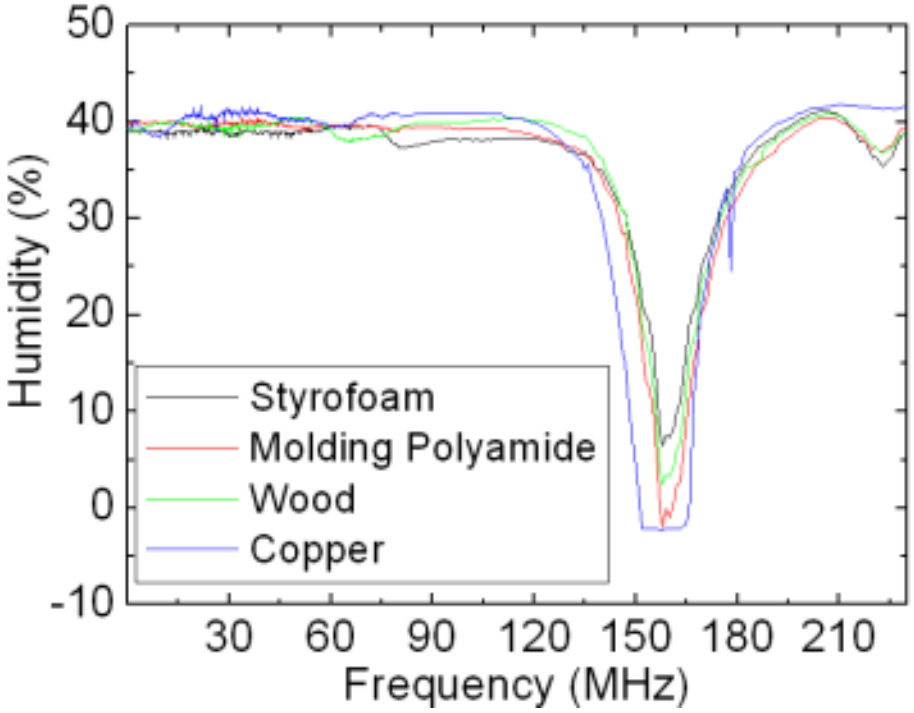

(d)

Figure 6. Results of thermo-hygrometer and supports with CDN (a) loop impedance values, (b) injected current, (c) temperature susceptibility level, (d) humidity susceptibility level.

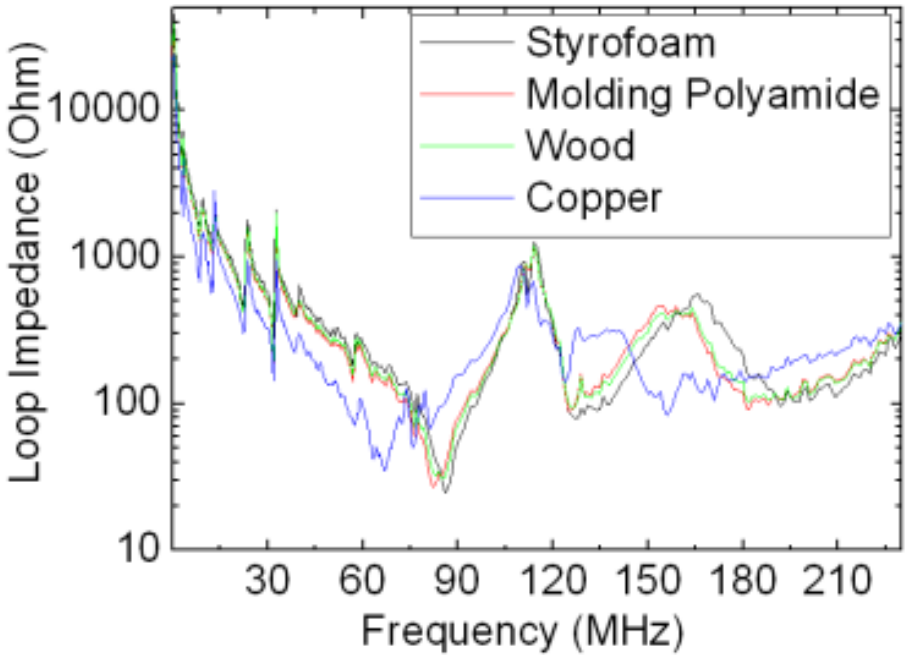
Loop Impedance (Ohm)
10000
1000
100
10
30
60
90
120
150
180
210
Frequency (MHz)
Styrofoam
Molding Polyamide
Wood
Copper

(a)

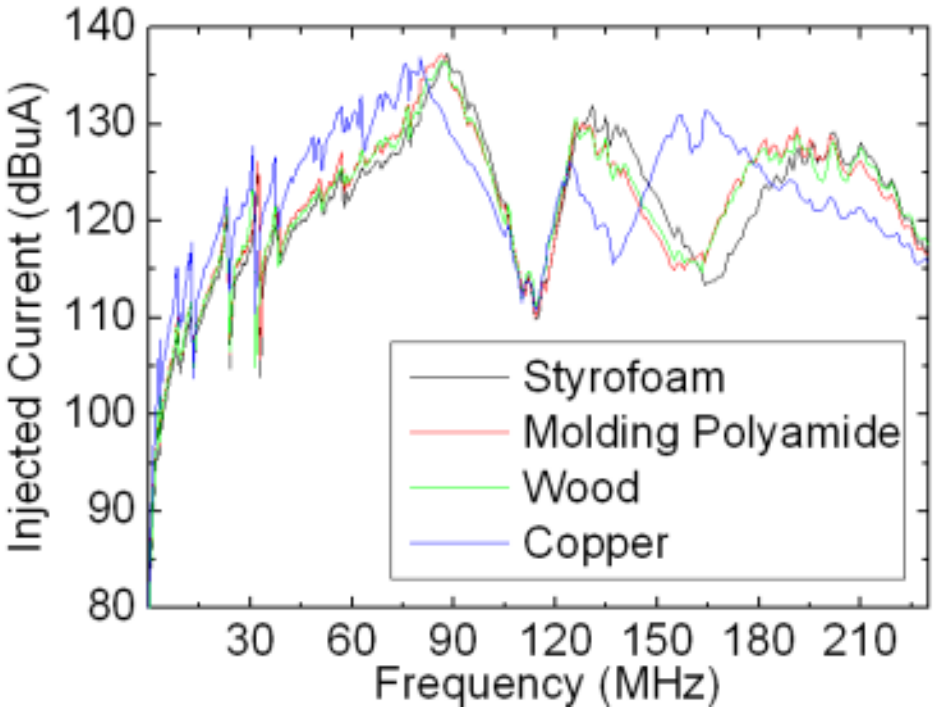
Injected Current (dBuA)
140
130
120
110
100
90
80
30
60
90
120
150
180
210
Frequency (MHz)
Styrofoam
Molding Polyamide
Wood
Copper

(b)

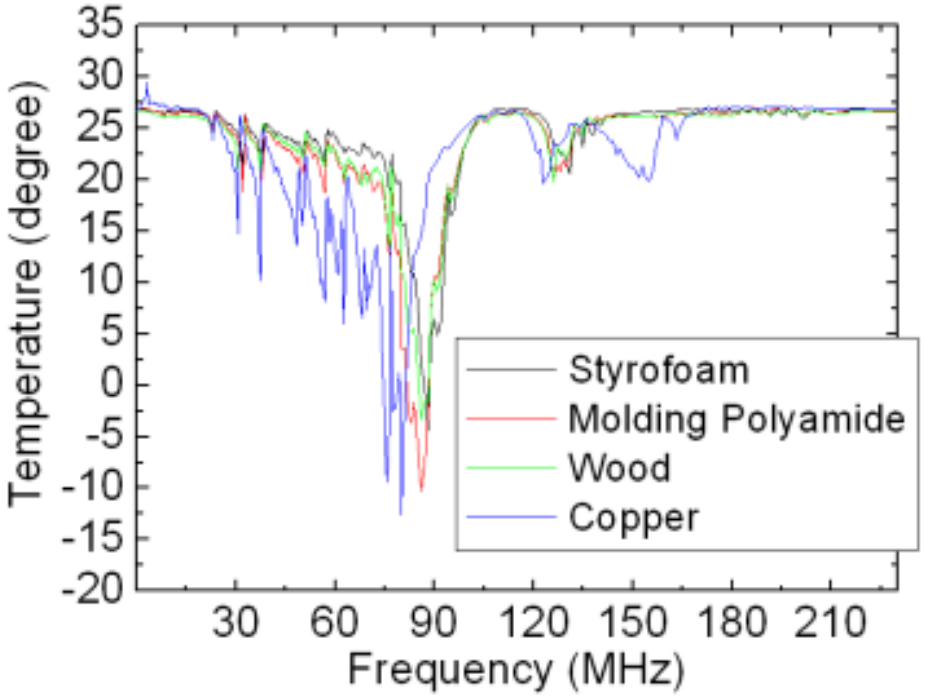

(c)

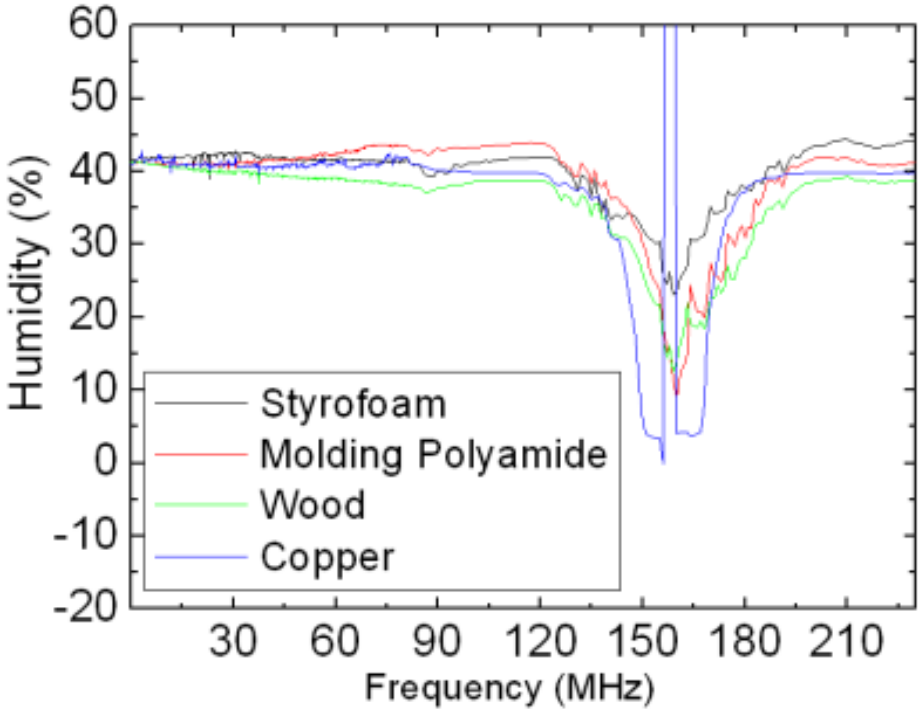

(d)

Figure 7. Results of thermo-hygrometer and supports along with connection to the mains without CDN (a) loop impedance values, (b) injected current, (c) temperature susceptibility level, (d) humidity susceptibility level.

After the testing with the CDN, finally, the results for the setup, in which the EUT was directly connected to the mains without a CDN, are similarly shown in Fig.7. Due to unpredictable and undulant impedance behaviour of the mains, the graphs are different from the graphs of the setup with the CDN. The removal of the CDN from the setup significantly changes the loop impedance and consequently, the injected current and the susceptibility levels. Despite this change, the relation between the loop impedance, the current and the susceptibility level remains consistent like in the case with the CDN. The graphs in Fig.7 also show again that the type of the used support appreciably affects the test results and may lead to variances in test results between laboratories.

Finally, the dielectric constant results of the samples acquired at 2 GHz in the measurement setup shown in Fig.4 are given in Table 1.

Table 1. Measured dielectric constant of samples.

Material	**Dielectric constant** (ε_r) **at 2 GHz**
Wood	1.91
Molding Polyamide	3.07
White styrofoam	1.02

3. RADIATED TESTS

a. Introduction

The radiated immunity and emissions measurement set-up considered in this study is according to CISPR25 [15] standard. The reason is that it is more suitable to produce higher differences due to the reduced distance between the reference on-table ground plane and the cables of the EUT. Moreover, it is a similar situation compared with the conducted immunity, as the cables are 5 cm above the ground plane, using a support material between the cables and the ground plane. On the other hand, in test according to the IEC 61000-4-3 standard, for on-table equipment, the distance between the ground plane and the EUT is 80 cm, using a table to place the equipment and isolation supports are not used. Hence, the research study is focused on the CISPR 25 measuring set-up.

b. Measurement setup

In Figure 8, the set-up defined at CISPR 25 standard can be observed.

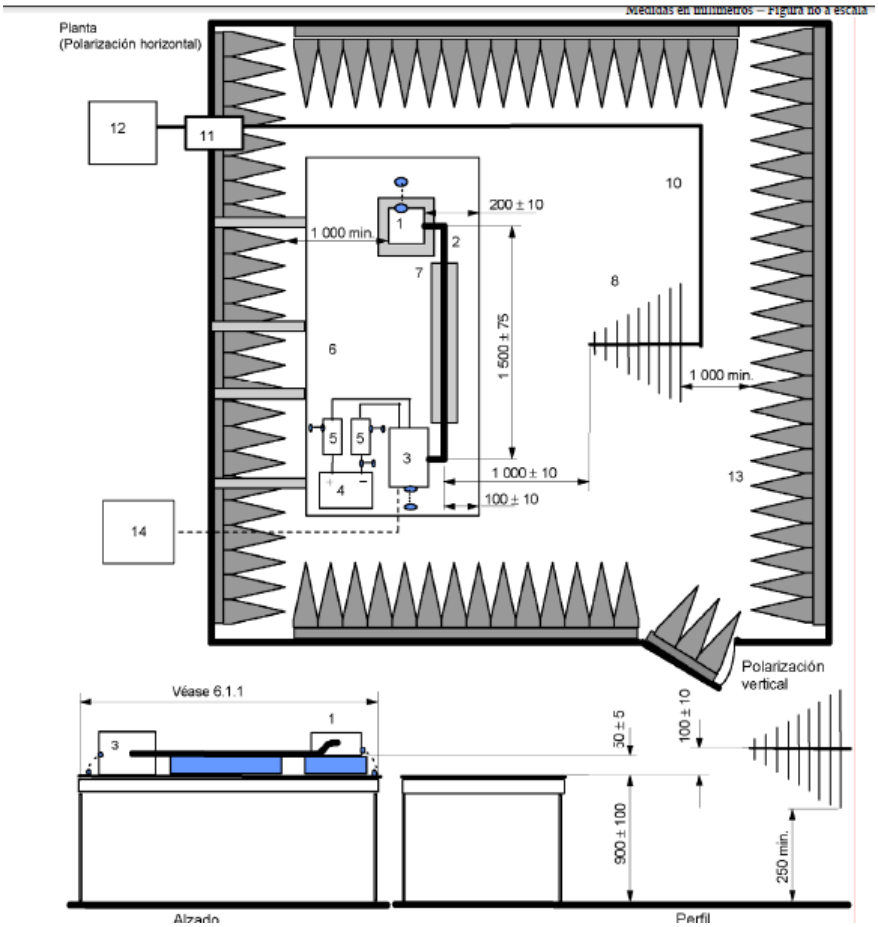

Figure 8. CISPR 25 test set-up definition.

A measurement is defined to obtain the transfer function [16] between the measuring Bilog antenna and the LISN output connected at the cables to measure the current couplet at the wires above the isolation material. Moreover, a biconic antenna is also placed to measure also the transfer function with the Bilog antenna in order to measure the electric field that will be incident when an EUT is placed over the isolation material. A diagram of the measurement is found in Figure 9.

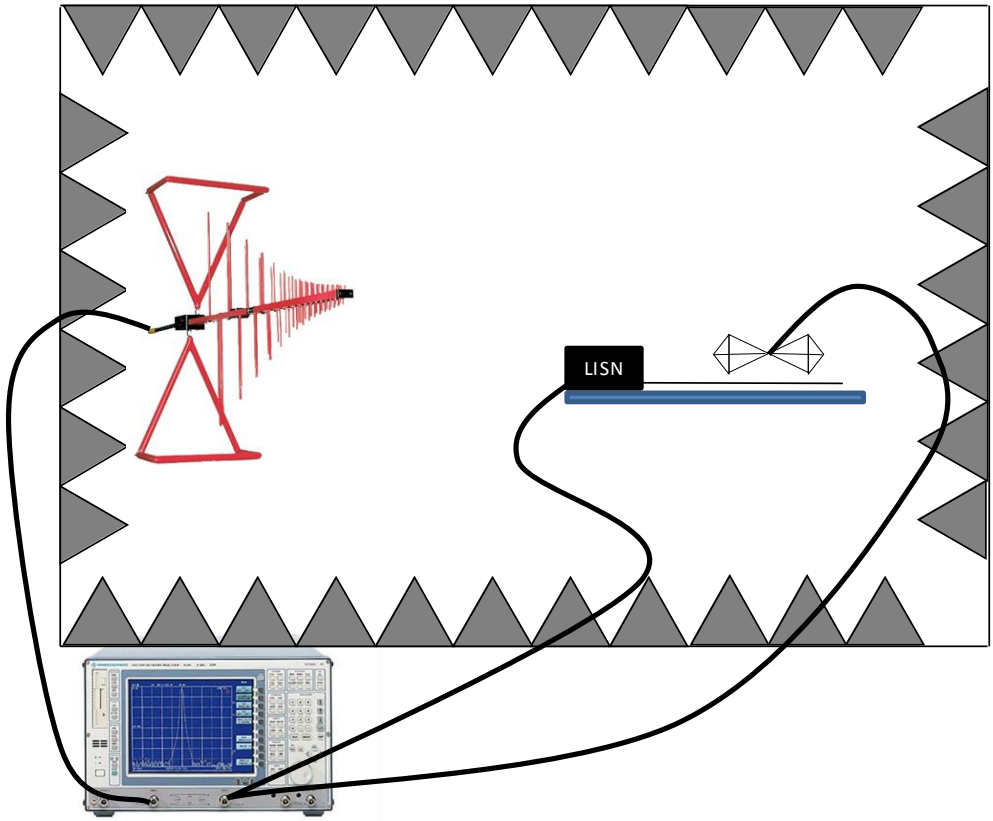

Figure 9. Measurement set-up to study the effect of the support materials according to CISPR25 for emissions and immunity tests.

In order to measure the transfer function a Rohde & Schwarz ZVRE VNA is employed. Port 1 is connected to the Bilog antenna and Port 2 is connected to the LISN output or the biconic antenna. The measurement is carried out with the Bilog antenna in vertical polarisation and the frequency range is defined between 20 MHz and 2 GHz. Although the frequency range of the LISN is limited to 110 MHz for EMI measurements, the frequency range has been extended in this study, as we want to compare the results given with different isolation materials. Performing relative measurements instead of absolute ones, as it is suitable for us just to identify the changes at the transfer function with the different isolation materials.

A view of the constructed set-up measured at the UPC anechoic chamber can be found in Figure 10 and Figure 11. While in Figure 10 it can be seen a view of the test set-up for the “Air” measurement, a close look of the set-up a Styrofoam placed can be seen in Figure 11.

Figure 10. A view of the test set-up for the “Air” measurement.

Figure 11. Close look of the set-up with a Styrofoam.

Regarding the materials employed in the measurements, three different Styrofoam are used (White, Square and Blue). This type of material is commonly employed for measurements, as it is introduced low deviations to the measurements.

Below, the Figure 12 with pictures with the different materials can be found.

“Air” measurement

White Styrofoam

Square Styrofoam

Figure 12. Styrofoam measurement set-up according to CISPR25.

c. Results

If the transfer function with the “air” measurement is compared to the three measurements with the Styrofoam, reduced differences are observed; when the transfer function of the LISN or the biconic antenna is observed.

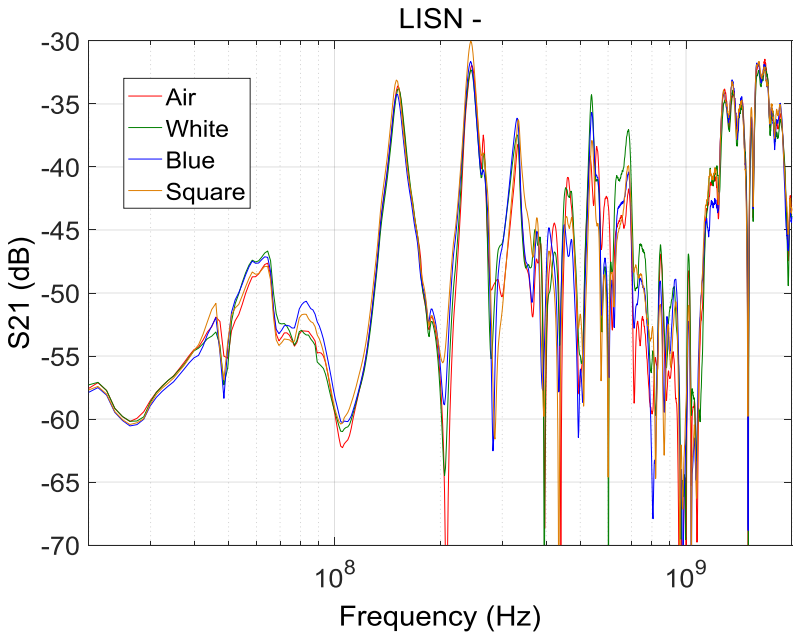

Figure 13. Transfer function between the Bilog antenna and the LISN comparison when the different Styrofoam materials are employed.

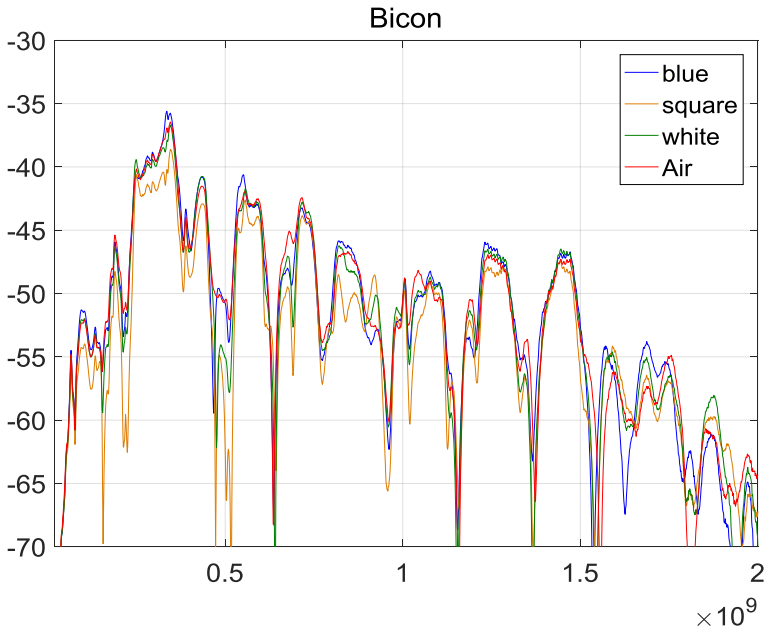

Figure 14. Transfer function between the Bilog antenna and the biconic antenna comparison when the different Styrofoam materials are employed.

Hence, we can conclude that the Styrofoam is a proper material to reduce the uncertainty in radiated emissions and immunity testing. There is not an observation of a significative frequency shift due to the support material and the amplitude differences in Figure 13 and 14 are attributable to the test repeatability as we need to mount and dismount the test set-up to exchange the isolation material. These slight differences are close to 2-3 dB.

Additionally, in order to complete the study, another measurement has been conducted with an unknown plastic material (Figure 15).

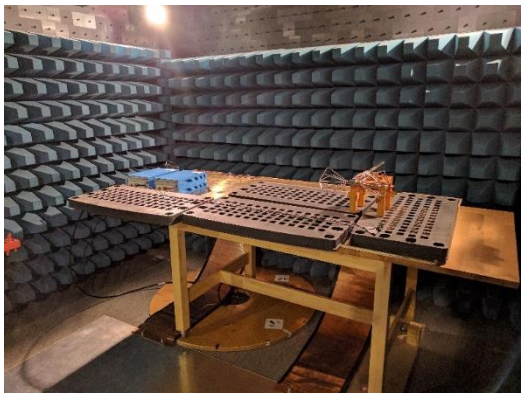

Figure 15. Unknown plastic material used as support material.

We repeat the same procedure than before and measure the transfer function. Results are shown in Figure 16.

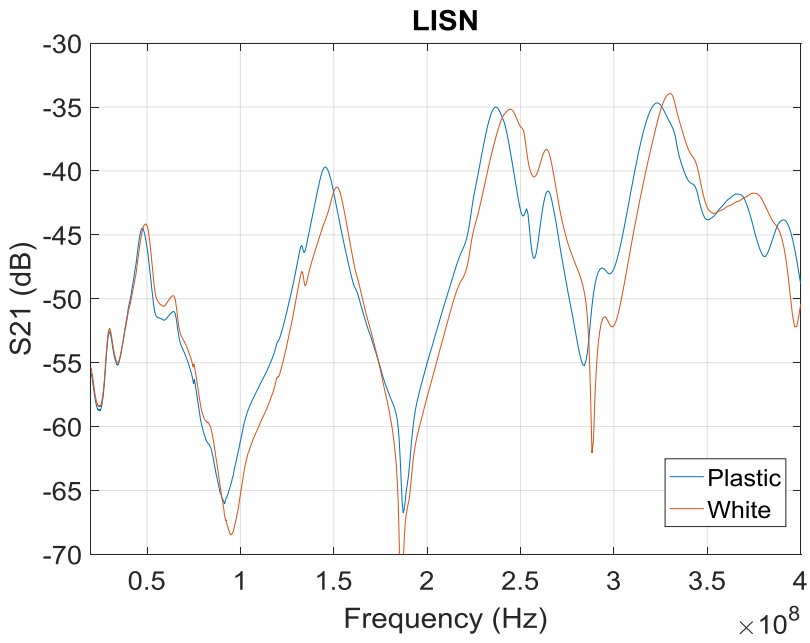

Figure 16. Transfer function between the Bilog antenna and the LISN when the unknown plastic material is employed.

In this occasion, a frequency deviation is observed due to the unknown plastic material. Therefore, from the emissions point of view, this can be critical for narrow band interferences as differences up to 6 dB can occur.

Finally, this study will be complemented with electromagnetic (EM) simulation, considering different type of materials like wood or Polyethylene.

4. EM SIMULATIONS

a. Simulated scenario

The aim of the EM simulations is to evaluate the influence of the support materials for radiated tests. As it has been explained before, the data obtained is useful for immunity and emissions tests set-up. Following the measurements carried out at the previous section, a simulation scenario according to CISPR 25 is defined.

At the model of the EM scenario, it is considered the measuring or transmitting antenna, the ground floor, the on table ground plane, the cables, the table, the support materials and the different loads (simulated as lumped elements). In Figure 17 there is a screenshot of the simulated model.

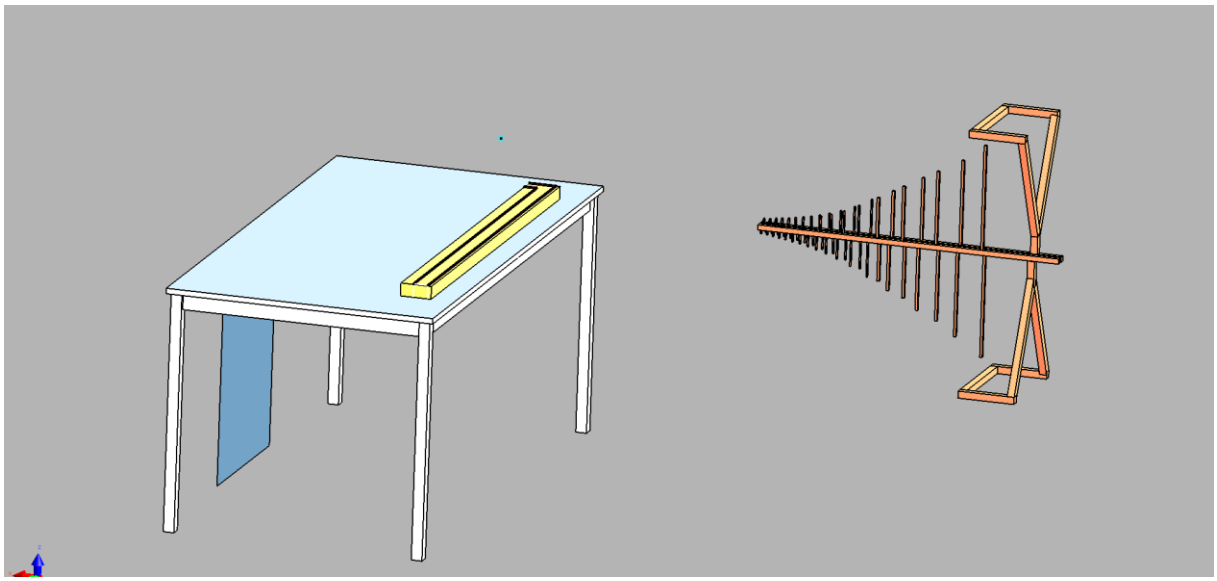

a)

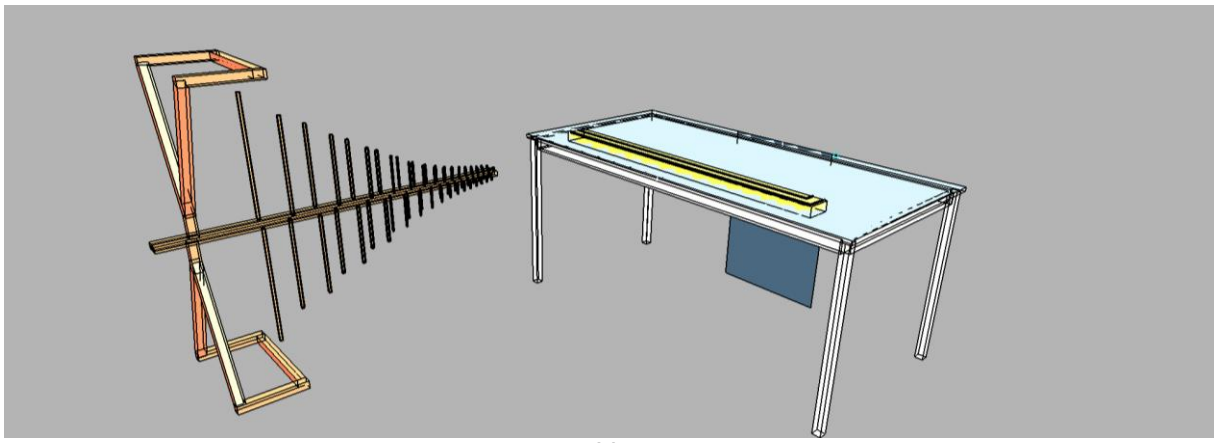

b)

Figure 17. EM simulation model according to CISPR 25 standard for radiated emissions and radiated immunity considering a Bilog antenna.

Regarding the set-up on the table, a schematic describing the elements can be found in Figure 18.

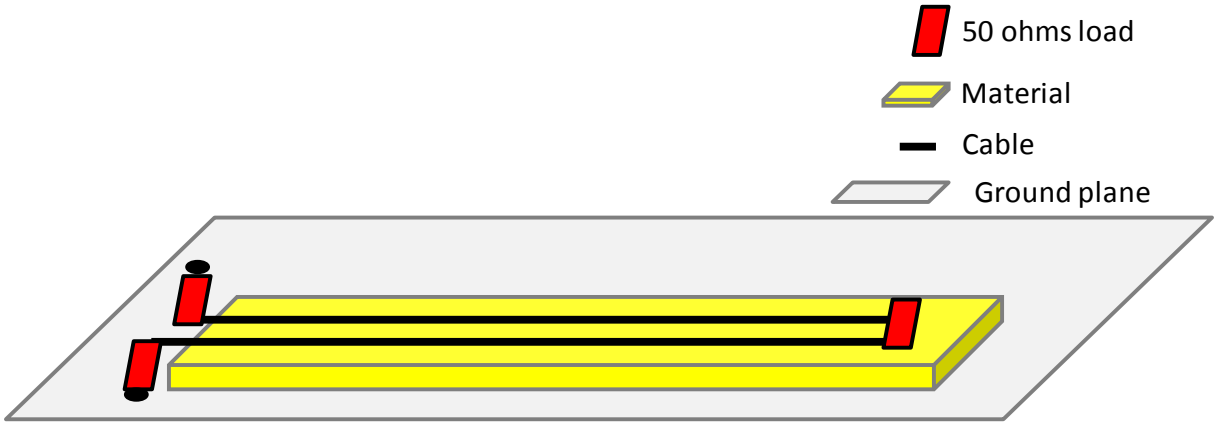

Figure 18. Schematic of the elements on the table, considering the ground plane, cables, ground plane and support material.

The 50 Ohms loads model the load between both wires, and the load that simulate the LISN at the left part of Figure 18. The ground plane is defined as Perfect Electric Conductor (PEC) as well as the wires. Concerning the support material, four different approaches have been considered in the simulation. In Table 2, the characteristics of the support materials evaluated are defined.

Table 2. Parameters of the different support material simulated.

Support material	Relative permittivity	Electric conductivity
Air	1	0
Styrofoam (Expanded Polyethylene)	1.03	1.717901e-5
Wood	2	1e-14
Polyethylene	2.25	0.0005

b. Simulation method

Finite-Difference Time-Domain (FDTD) EM simulation method has been selected according to several benefits that introduce us compared with other EM simulation methods particularly for EMC applications [17, 18, 19, 20]. This numeric method is one of the most used in EMC applications as FDTD gives us broadband. FDTD allows us to produce in a single simulation all the frequency range that it is defined at the EMC standard. This is a great advantage if we compare FDTD method to other EM simulation methods, which many of them need a simulation for each frequency to evaluate.

Regarding the method itself, it is a 3D numerical method capable of calculating the magnetic and electric field. FDTD proposed by Yee in 1966 is a direct solution of Maxwell's curl equations in the time-domain. The electric and magnetic field components are allocated in space on a discrete mesh of a Cartesian coordinate system. The E- and H-field components are computed each time-step using the finite-difference by means of the second order approximation of Maxwell equations.

c. EM Simulation parameters and hardware

The simulation software employed for the EM simulation [21] is Sim4Life v3.4, which allows us to conduct the FDTD simulation. The hardware used is a Personal Computer (PC), with an Intel® core ™ i7-7700 CPU @ 3.6 GHz with 16 GB of RAM memory.

For each of the different materials simulated two different simulations have been launched in order to obtain the transfer function of the model. This multi-port simulation is executed when the source is at the antenna and when the source is at the 50 Ohm load corresponding to the LISN. Regarding the source, of the simulation, an edge source is defined with a Gaussian pulse with spectral content from 10 MHz up to 1 GHz (Figure 19). This is the limit frequency as there are some limitations with the material database and with the hardware of the PC.

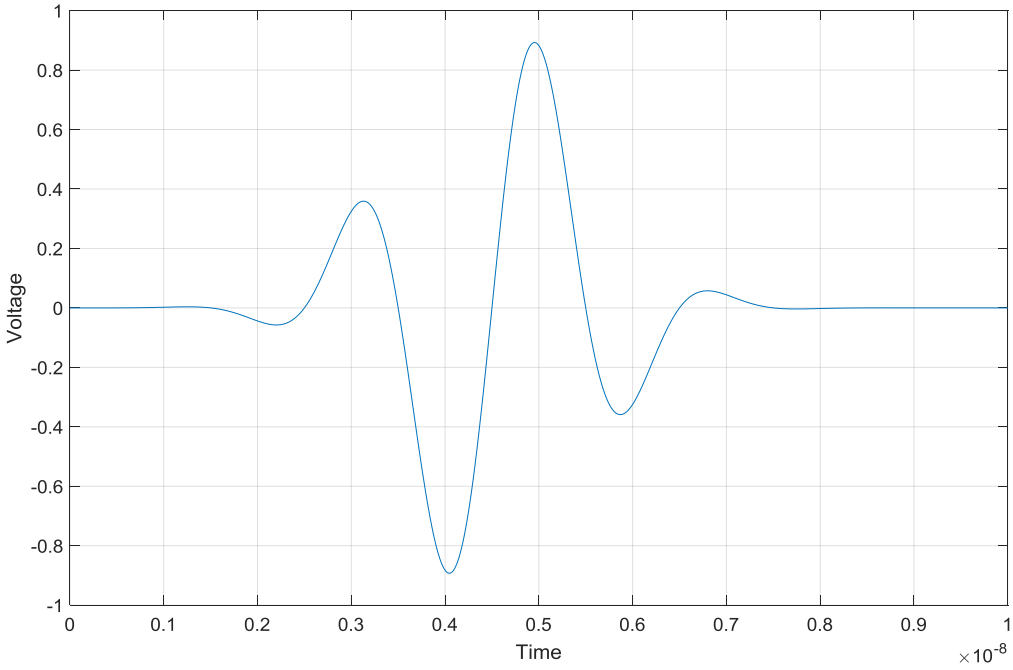

Figure 19. Source waveform.

Concerning the discretization, the space is discretized with 70.02 MCell and the simulation step is 1.2207e-11. Finally, the total simulated time is 50 ns. In Figure 20, the discretization of the antenna can be observed.

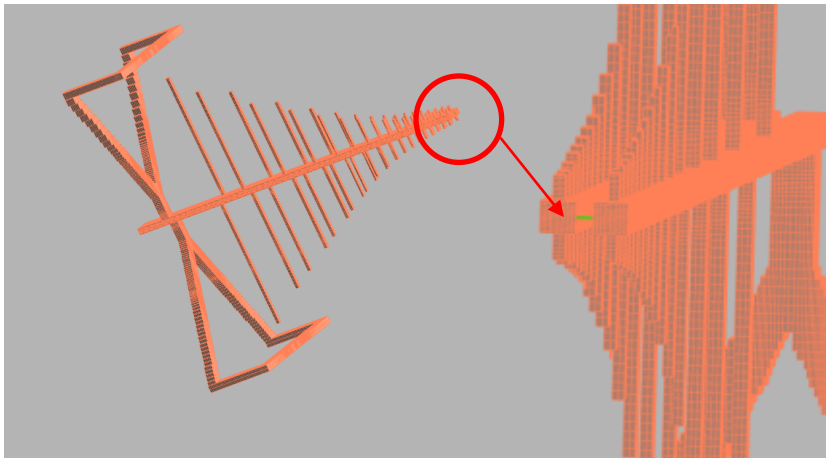

Figure 20. Antenna discretization.

Otherwise, the time needed to carry out each simulation is 5 h 30 minutes, reaching a speed of 97 MCell/s.

d. Simulation results

In this section, the results of the scenarios model with the four different support materials are shown. The results show the transfer function between the antenna and the load, which simulates the LISN, to compare with the previous done measurements. It is important to highlight that using the EM simulation parasitic effects from the measurement like the cables effect disappear. Being able to analyse exclusively the impact of placing different support materials.

In Figure 21, the data of the different materials can be observed. From the simulation results several conclusions can be done. Firstly, the agreement between the Air material and the Styrofoam is extremely good. Concluding that the impact of placing the Styrofoam is almost negligible to the uncertainty budget. Otherwise, when the air situation is compared with the wood or the Polyethylene large differences are observed at the level and the shape of the transfer function.

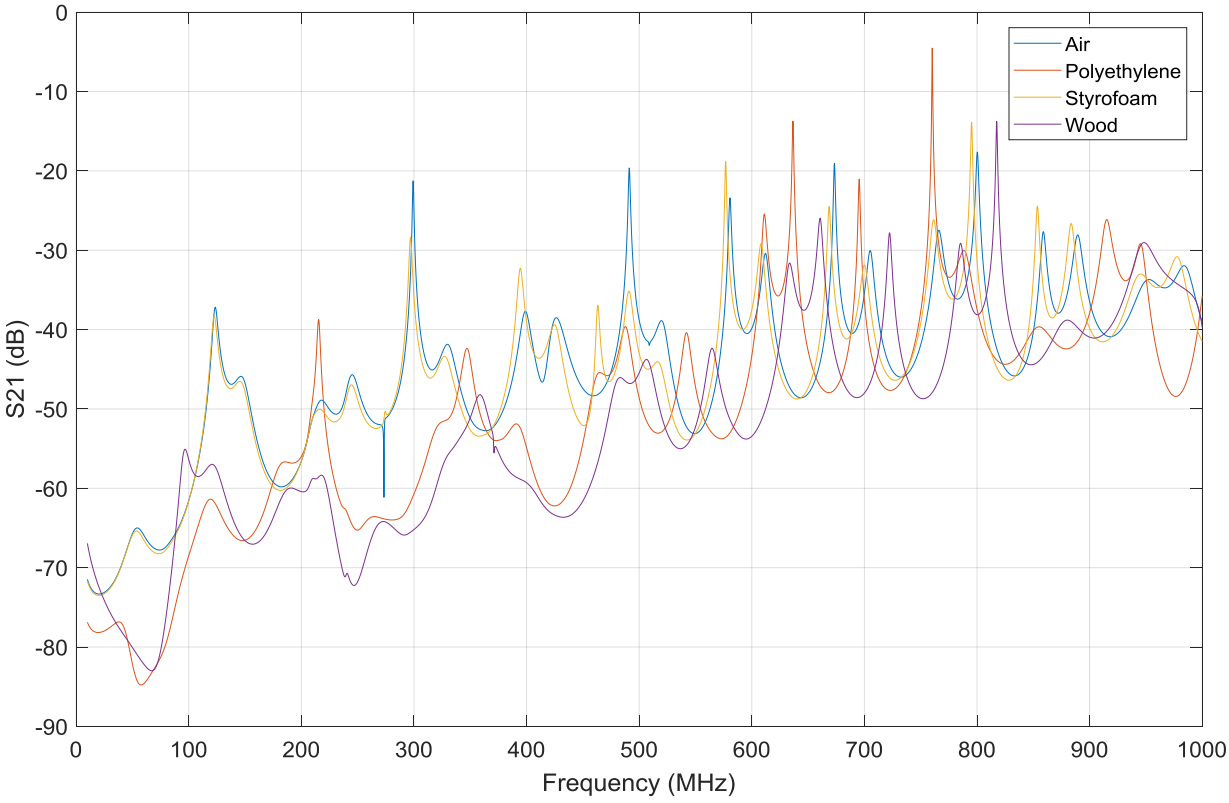

Figure 21. Comparison of the transfer function obtained when the different support materials are considered.

Following, the comparison between the air and the Styrofoam is shown in Figures 22 and 23. Showing the good agreement but also observing a frequency displacement of the peaks up to 5 MHz for frequencies close to 1 GHz.

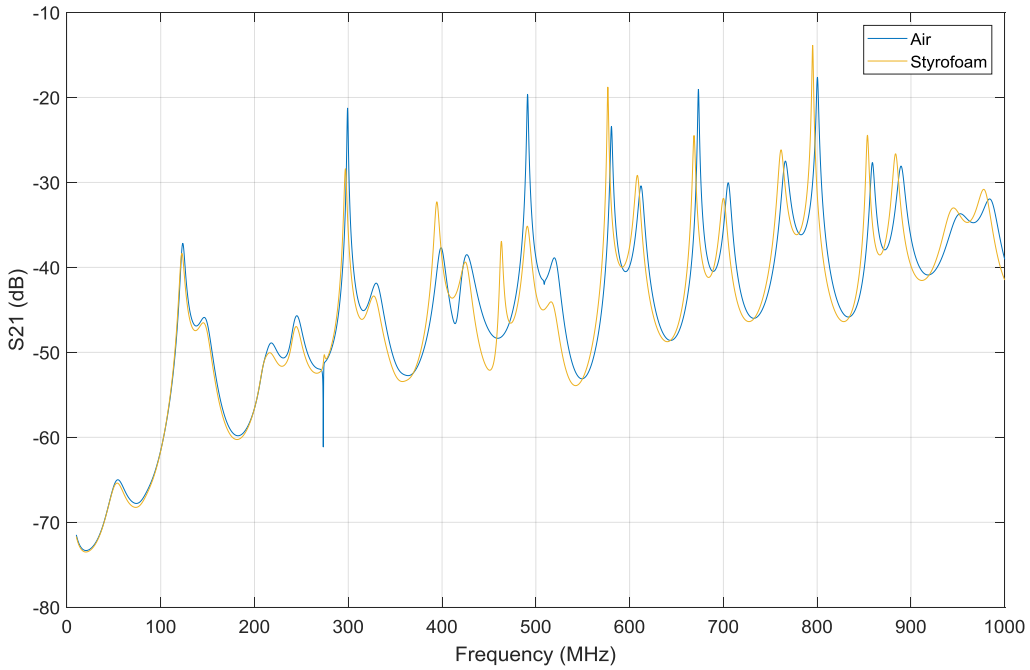

Figure 22. Comparison of the transfer function obtained when the Air and the Styrofoam are considered.

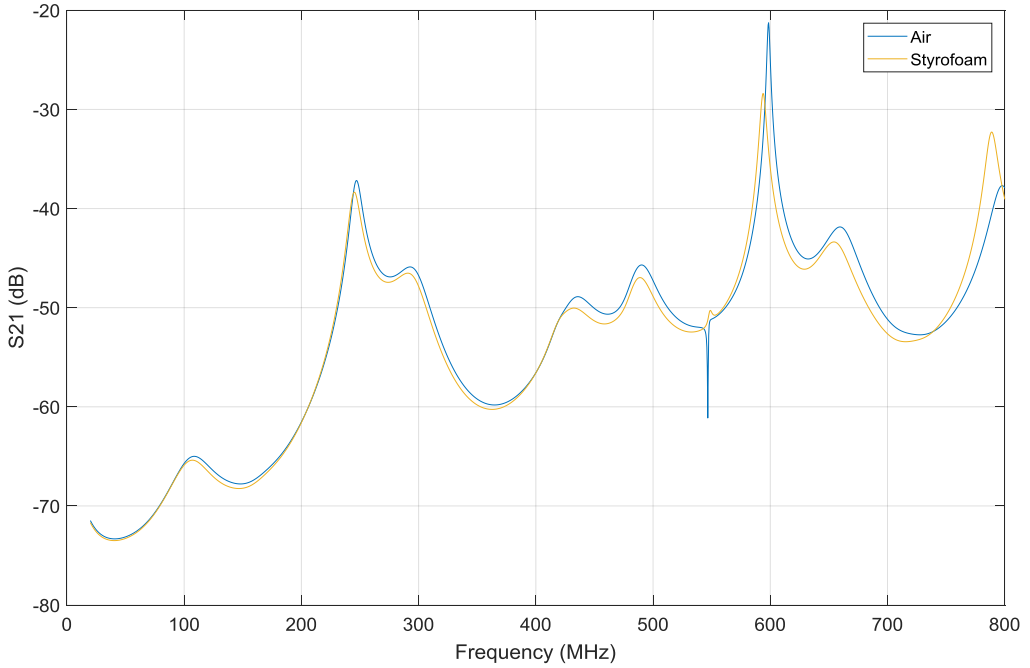

Figure 23. Zoom of the comparison of the transfer function obtained when the Air and the Styrofoam are considered.

Finally, in Figure 24,

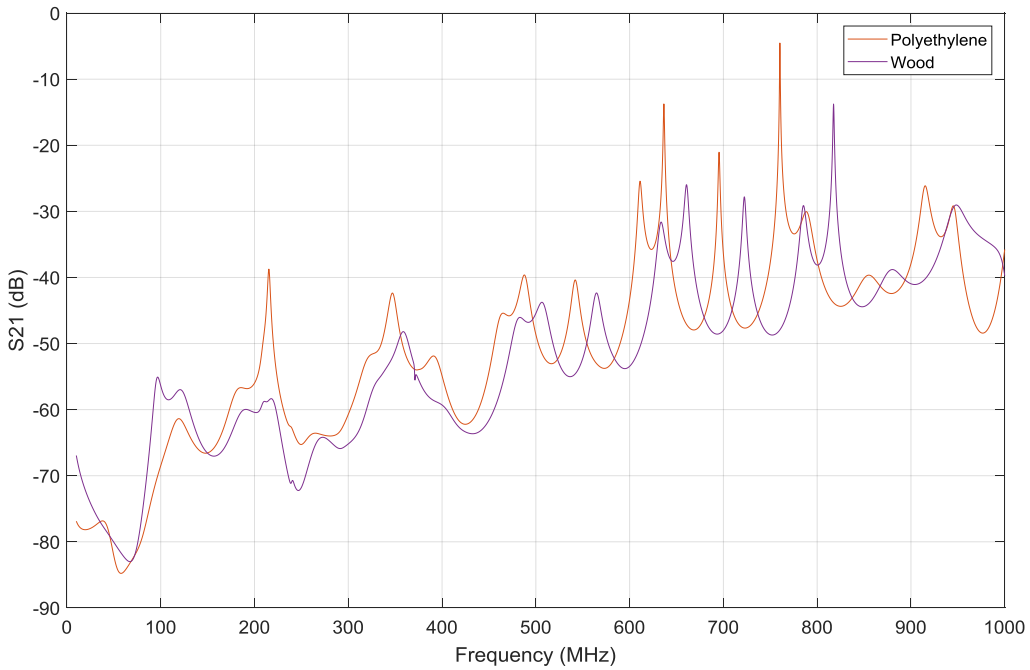

Figure 24. Zoom of the comparison of the transfer function obtained when the Air and the Styrofoam are considered.

According to the EM simulation the support material of the cables have a huge impact to the transfer function, supposing an extremely critical element to the uncertainty budget. The transfer function changes the shape and the level, therefore, differences larger than 10 dB are observed, when materials with an electric permittivity between 1 and 2.25 are evaluated. Moreover, the effect of the frequency displacement is also observed for materials close to the Air properties.

5. CONCLUSION

In this work, the influence of supports commonly used on conducted immunity and conducted emission EMC tests was measured along with loop impedance values and induced currents. Although many types of dielectric materials are utilized in conducted immunity and conducted emission measurements on account of the fact that they are just non-metallic, some of them give unacceptable uncertainty contribution to measurement results. The measurement results in this research reveal that the use of the styrofoam type supports in conducted immunity and conducted emission tests leads to the minimum measurement errors and consequently minimum uncertainty level.

In addition to conducted immunity and emission tests, in this work, the influence of supports was studied for radiated emission and immunity tests. In this context, we can conclude that the Styrofoam is a material which also introduces low uncertainty to the radiated emissions and immunity tests. On the other hand, if other materials like wood or polyethylene are used a huge impact to the transfer function and the emissions and immunity tests is clearly observed.

6. REFERENCES

[1] IEC61000-4-6, Electromagnetic compatibility (EMC) - Part 4-6: Testing and measurement techniques - Immunity to conducted disturbances, induced by radio-frequency fields.

[2] Tim Williams, Stan Baker, “Main Report - Uncertainty of immunity measurements”, DTI-NMSPU project R2, Online:http://www.elmac.co.uk/r22b1/R22b1_mainrept.pdf.

[3] Tim Williams, Stan Baker, “Pitfalls and practice of IEC 61000-4-6”, DTI-NMSPU project R2, Online:http://www.elmac.co.uk/pdfs/PNP_61000-4-6.pdf.

[4] K. Mourougayane, S. Karunakaran, P. Satheesan, P.K Sivakumar, “Automation of EMC tests - Software development and system integration approach”, INCEMIC 9th International Conference on Electromagnetic Interference & Compatibility, Bangalore, India, pp. 349 - 352, 23-24 Feb. 2006.

[5] D.Pommerenke, “Methods for speeding up radiated and conducted immunity tests”, IEEE International Symposium on Electromagnetic Compatibility, Washington, DC, USA, vol. 2, pp. 587 - 592, 21-25 Aug. 2000.

[6] R. Heinrich, “Investigation and comparison of different methods for EM clamp calibration”, APEMC Asia-Pacific Symposium on Electromagnetic Compatibility, Beijing, China, pp. 990 – 993, 12-16 April 2010.

[7] G. Mahesh, B. Subbarao, “Comparison of Bulk Current Injection test methods of automotive, military and civilian EMC standards”, INCEMIC 10th International Conference on Electromagnetic Interference & Compatibility, Bangalore, India, pp. 547 - 551, 26-27 Nov. 2008.

[8] J. Sroka, “Practical approach to IEC 61000-4-6 testing”, IEEE International Symposium on Electromagnetic Compatibility, Minneapolis, MN, USA, vol. 1, pp. 367 - 370, 19-23 Aug. 2002.

[9] R. Sivaramakrishnan, S. Santhakumari, R. Dhivya, S. Parthiban, L.N Charyulu, “Conducted RF immunity testing - Observed variation in the injected current”, INCEMIC 10th

International Conference on Electromagnetic Interference & Compatibility, Bangalore, India, pp. 243 - 245, 26-27 Nov. 2008.

[10] Soydan Çakır, Osman Sen, Savas Acak, Marco Azpúrua, Ferran Silva, Mustafa Çetintas, “Alternative Conducted Immunity Tests”, IEEE Electromagnetic Compatibility Magazine, vol.5, issue.3, pp 45-51, 2016.

[11] Soydan Çakır, Osman Şen, Savaş Acak, Mustafa Çetintaş, “Alternative conducted immunity testing with multiple CDNs and wire winding”, IEEE International Symposium on Electromagnetic Compatibility (EMC), pp 1260-1260, August 2016.

[12] Osman Sen, Soydan Cakir, Murat Celep, Mehmet Cinar, Ramiz Hamid, Mustafa Cetintas, “Influence of dielectric support on military radiated emission tests above 30 MHz”, Asia-Pacific International Symposium on Electromagnetic Compatibility (APEMC), 2016.

[13] Tarateeraseth V., Bo Hu; Kye Yak See, Canavero F.G., “Accurate Extraction of Noise Source Impedance of an SMPS Under Operating Conditions”, IEEE Transactions on Power Electronics, Vol. 21, No.1,pp. 111-117, Jan 2010.

[14] A. M. Nicolson and G. F. Ross, “Measurement of the intrinsic properties of materials by time-domain techniques,” IEEE Trans. Instrum. Meas., vol. IM-19, no. 4, pp. 377–382, Nov. 1970.

[15] “CISPR 25: Limits and methods of measurement of radio disturbance characteristics for protection of receivers used on board vehicles,” IEC.

[16] A. Radchenko, V. Khilkevich, N. Bondarenko, D. Pommerenke, M. Gonser, J. Hansen, C. Keller, "Transfer Function Method for Predicting the Emissions in a CISPR-25 Test-Setup," in Electromagnetic Compatibility, IEEE Transactions on , vol.56, no.4, pp.894-902, Aug. 2014 doi: 10.1109/TEMC.2013.2297303.

[17] I. Oganezova, R. Kado, B. Khvitia, A. Gheonjian, R. Jobava, "Simulation of conductive and radiated emissions from a wiper motor according to CISPR 25 standard," in Electromagnetic Compatibility (EMC), 2015 IEEE International Symposium on , vol., no., pp.963-968, 16-22 Aug. 2015 doi: 10.1109/ISEMC.2015.7256296.

[18] M. Gonser, C. Keller, J. Hansen, V. Khillkevich, A. Radchenko, D. Pommerenke, and R. Weigel, “Simulation of automotive EMC emission test procedures based on cable bundle measurements,” in Proc. IEEE MTT-S Int. Microw. Symp. Dig., 2012, pp. 1–3.

[19] R. Jauregui, M. Pous, Y. Vives, M. Fernandez, P.J. Riu, and F. Silva. Car windshield behavior transient analysis by FDTD. In Electromagnetic Compatibility - EMC Europe, 2009 International Symposium on, pages 1-4, June 2009. doi: 10.1109/EMCEUROPE.2009.5189718.

[20] D. Prost, F. Issac, T. Volpert, W. Quenum, and J.-P. Parmantier, “Lightning-Induced Current Simulation Using RL Equivalent Circuit: Application to an Aircraft Subsystem Design” Electromagnetic Compatibility, IEEE Transactions on, 55(2):378-384, April 2013.

[21] Sim4life. 3D Electromagnetic Full wave simulation software. http://www.zurichmedtech.com/sim4life/physics-models/p-em-fdtd/.